LETTERS
PUBLISHED ONLINE: 6 DECEMBER 2009 | DOI: 10.1038/NGEO708
nature geoscience

Towards absolute plate motions constrained by lower-mantle slab remnants

Douwe G. van der Meer[1,2]*, Wim Spakman[1]*, Douwe J. J. van Hinsbergen[1,3,4], Maisha L. Amaru[1,5] and Trond H. Torsvik[3,4,6]

Since the first reconstruction of the supercontinent Pangaea, key advances in plate tectonic reconstructions have been made[1–6]. Although the movement of tectonic plates since the start of the mid-Cretaceous period (~100 million years (Myr) ago) is relatively well understood[1,2], the longitudinal position of plates before this period is not constrained at all. Here, we use a global mantle tomography model[7] to estimate the longitude of past oceanic subduction zones. We identify 28 remnants of oceanic plates that were subducted into the lower mantle and link these to the mountain building zones from which they are likely to have originated. Assuming that these remnants sank vertically through the mantle, we reconstruct the longitude at which they were subducted. Our estimates for the location of the subduction zones are offset by up to 18° compared with plate tectonic reconstructions for the corresponding period. We did not detect oceanic plate remnants from the Carboniferous period (~300–360 Myr ago), or before, suggesting that the tomographic visibility of subduction is limited to the past 300 Myr.

Since the first qualitative plate reconstruction of the supercontinent Pangaea was determined by fitting palaeoclimatic belts and modern continental margins, key advances in plate reconstructions have been made with the development and use of palaeomagnetic apparent polar wander paths, ocean floor magnetic anomalies and hotspot reference frames[1,2], leading to global plate tectonic reconstructions[3,5,6]. Absolute plate motion models have often been based on assumed hotspot fixity and are well constrained only up to the Cretaceous period owing to the lack of any preserved older oceanic hotspot tracks[1,2]. These, and other models, offer no control on absolute palaeolongitude before the Cretaceous.

Seismic tomography studies of the mantle have allowed for increasingly detailed correlations between deep mantle structure, mostly focused on presumed remnants of subducted plates and plate tectonic evolution[8–16]. This, however, has not led to strong constraints on absolute plate motion. Recently, correlations between deep, presumably hot and dense mantle heterogeneities at the core–mantle boundary and large igneous provinces were obtained from a plate reconstruction[3,4], leading to possible predictions of absolute palaeolongitude for the entire Phanerozoic eon[17]. This reconstruction model, however, assumes zero longitude motion for Africa before the Cretaceous.

Here, independently of any reconstruction model, we carry out a global interpretation of positive seismic anomalies in the lower mantle based on the assumptions that these reflect relatively cold remnants of subducted lithosphere[8–16], and that slabs, once detached, sink more or less vertically in the mantle[8–10,18] marking the location of their former subduction zones. Geological evidence for former subduction is constituted by orogens created in plate convergence zones, often comprising the remnants of a volcanic arc. Studies comparing the amount of Tethyan subducted material predicted by geological reconstructions with volumes of subducted lithosphere imaged in the mantle by seismic tomography[11,12] suggest a first-order correlation between the onset and end of subduction and the onset and end of orogenesis, respectively. In line with this inference, we assume that to first order, the age of the base and top of a lower-mantle slab can be correlated in time with the onset and end, respectively, of the associated orogeny. Timing errors of the order of 10–25 Myr are inferred from the geological literature used for interpretation[5,19–21] (Supplementary Information) and include uncertainties in upper-mantle subduction history.

Using this rationale, we interpret lower-mantle slab remnants from the tomographic model UU-P07 (ref. 7), the successor of BSE98 (ref. 22), and correlate these with their corresponding orogenies. Identification, depth of top and bottom, timing and images (Supplementary Figs S1–S28) of slab remnants are documented extensively in the Supplementary Information. The Farallon, Mongol-Okhotsk and Aegean Tethys slabs have already been studied extensively and correlated to geologic events and act here as anchor points for the global interpretation of the lower mantle. The still-subducting Aegean Tethys slab remnant was shown to reach a depth of ~2,000 ± 100 km (refs 11, 12, 22; Supplementary Fig. S1). The onset of subduction in the Aegean region is inferred to approximate 171±5 Myr, as represented by metamorphic soles below the oldest Aegean ophiolites[23]. The Mongol-Okhotsk slab remnant is located below northern Siberia from the base of the mantle up to mid-mantle (Supplementary Fig. S2) and subducted in the Middle Triassic/Middle Jurassic[5,9,19]. The Farallon slab remnant[8] is located below eastern Laurentia from the deep lower mantle to the upper part of the lower mantle (Supplementary Fig. S3). The slab has been interpreted to represent eastward-subducted Farallon oceanic lithosphere, but estimates of the start of subduction of the slab vary from Late Cretaceous[8] to Late Jurassic[13]. However, the geological record proves that subduction at the western continental margin of Laurentia initiated earlier, in the Early Jurassic[20,24]. This is adopted here as the start of subduction and related to the deepest part of the Farallon slab remnant. In the upper mantle the Farallon slab disintegrates into smaller fragments, which have been associated with subduction during the

[1]Institute of Earth Sciences, Utrecht University, Budapestlaan 4, 3584 CD Utrecht, The Netherlands, [2]Shell International Exploration and Production, Kesslerpark 2, 2288 GS Rijswijk, The Netherlands, [3]Center for Geodynamics, Geological Survey of Norway (NGU), Leiv Eirikssons vei 39, NO-7491 Trondheim, Norway, [4]Physics of Geological Processes, University of Oslo, NO-0316 Oslo, Norway, [5]Chevron Energy Technology Company, 250 St Georges Terrace, Perth, Western Australia 6000, Australia, [6]School of Geosciences, University of the Witwatersrand, WITS 2050 Johannesburg, South Africa.
*e-mail: douwe.vandermeer@shell.com; wims@geo.uu.nl.

Table 1 | Slab data set.

				Slab depth				Slab age				Slab midpoint			
				Base		Top		Base		Top					
Abbreviation	Slab name	Domain	Category	Min.	Max.	Min.	Max.	Min.	Max.	Min.	Max.	Depth	Age	Long. (°)	Lat. (°)
Aeg	Aegean Tethys	Tethyan	1	2,100	1,900	0	0	176	166	0	0	1,000	86	26	42
Far	Farallon	Laurentian	1	2,650	2,480	920	710	207	180	70	50	1,690	127	−75	34
MO	Mongol-Okhotsk	Cathaysian	1	2,900	2,815	1,900	1,700	240	230	180	155	2,329	201	76	67
Ag	Algeria	Tethyan	2	2,300	2,100	1,500	1,325	180	155	155	131	1,806	155	8	21
Al	Aleutian	Laurentian	1	810	710	0	0	84	52	0	0	380	34	−165	57
At	Atlantis	Laurentian	3	2,900	2,815	2,650	2,480	290	280	230	210	2,711	253	−39	22
Ba	Balkan	Other	3	2,900	2,815	2,650	2,480	280	260	220	200	2,711	240	17	47
Bf	Beaufort	Laurentian	3	2,650	2,480	2,300	2,100	230	208	163	144	2,383	186	−128	72
Ca	Caribbean	Laurentian	1	810	710	0	0	72	59	0	0	380	33	−63	13
CC	Central China	Cathaysian	2	2,900	2,815	1,500	1,325	260	250	121	84	2,135	179	88	45
Ch	Chukchi	Laurentian	3	1,900	1,700	1,325	1,175	163	144	120	100	1,525	132	170	77
EC	East China	Cathaysian	2	2,900	2,815	1,900	1,700	253	243	163	153	2,329	203	128	43
Eg	Egypt	Tethyan	3	1,500	1,325	920	810	121	84	84	70	1,139	90	26	19
GI	Georgia Islands	Other	3	2,900	2,815	2,100	1,900	295	285	220	190	2,429	248	−30	−57
Hi	Himalayas	Tethyan	2	1,175	1,040	500	440	84	79	43	20	789	57	78	26
Id	Idaho	Laurentian	2	2,480	2,300	920	810	208	163	100	84	1,628	139	−118	49
Kc	Kamchatka	Cathaysian	1	920	810	0	0	100	84	0	0	433	46	155	55
Mc	Manchuria	Cathaysian	1	920	810	0	0	110	50	0	0	433	40	135	46
Md	Maldives	Tethyan	2	2,300	2,100	920	810	220	200	70	57	1,533	137	79	14
Me	Mesopotamia	Tethyan	2	2,300	2,100	1,175	1,040	220	200	84	70	1,654	144	46	33
Mg	Mongolia	Cathaysian	2	1,900	1,700	1,175	1,040	193	163	120	100	1,454	144	118	48
NP	North Pacific	Other	3	1,700	1,500	810	710	140	110	110	80	1,180	110	−143	56
Ro	Rockall	Other	3	2,900	2,815	2,650	2,480	280	260	230	220	2,711	248	−13	57
Sa	Sakhalin	Cathaysian	2	1,175	1,040	810	710	100	84	84	52	934	80	149	53
So	Socorro	Laurentian	2	2,100	1,900	1,020	920	208	163	100	84	1,485	139	−108	17
TA	Trans Americas	Laurentian	2	2,900	2,815	2,480	2,300	230	208	193	163	2,624	199	−88	−2
Ve	Venezuela	Laurentian	2	1,500	1,325	810	710	118	110	72	59	1,086	90	−67	2
Wc	Wichita	Laurentian	2	2,815	2,650	2,100	1,900	230	208	193	163	2,366	199	−95	35

The slabs that are discussed in this letter are shown in bold. For a detailed overview, see the Supplementary Information and Supplementary Figs S1–S28.

Laramide orogeny (80–40 Myr) to present[13,25]. The total slab data set (Table 1, Supplementary Information), covers about half of the imaged positive wave-speed anomalies. For the remainder, notably in the deep mantle of the Indian and Pacific oceans, we could not date the slab remnants with the geological literature, or the tomographic model resolution was insufficient to warrant a useful quantitative interpretation.

Plotting the depths of the top and bottom of all slab remnants against the corresponding tectonic ages (Fig. 1) demonstrates an average slab sinking velocity in the lower mantle of 12 ± 3 mm yr^{-1}. This result is obtained independent of mantle rheology and thus can serve as a new constraint in the determination of lower-mantle viscosity. The sinking rate is slower than inferred by mantle flow estimates using Mesozoic–Cenozoic subduction models[18,26], which depend on assumed mantle rheology, but in agreement with other tomographic interpretations of 1–2 cm yr^{-1} (refs 10, 12, 14). Figure 1 shows that within the uncertainty estimates, the timing of palaeo-subduction can vary by ±25 Myr from the average, and slab remnants from palaeosubduction of any given age can be found ±300 km from the corresponding average depth. Here we are primarily concerned with first-order inferences on palaeolongitude and lower-mantle sinking rates on a global scale.

We find that all slab remnants in the lowermost mantle correspond to subduction systems of Triassic–Permian age (Fig. 1). No geological argument is found for correlating the deepest positive wave-speed anomalies to Carboniferous, or older subduction systems. We infer that the tomographic visibility of subduction history may be restricted to the past ~300 Myr of Earth evolution.

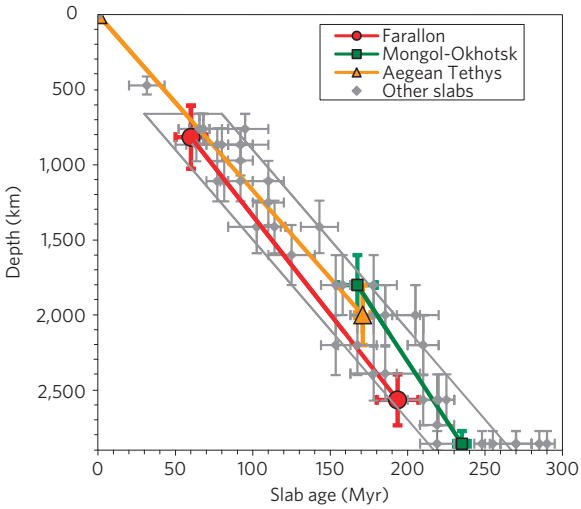

Figure 1 | Age–depth curve of interpreted slabs. The symbols indicate slab limits, with error bars in age–depth interpretation. The grey box represents average sinking rate (~12 mm yr^{-1}). The colour-coded slabs are previously described marker slabs.

Using seismic-anomaly survival times, defined as a 50–100 °C temperature anomaly, from a recent study[27], a slab maximum survival time of 300 Myr for slabs may indicate an increase in lower-mantle viscosity by a factor 100–300 relative to the upper

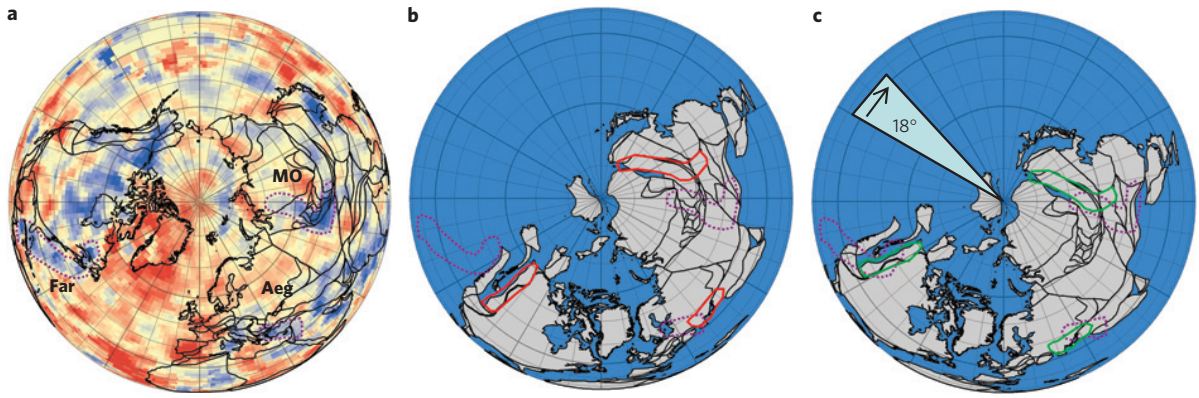

Figure 2 | Spatial longitude correction. North Pole orthographic projections. **a**, Tomographic depth slice[7] at 1,900 km, colour scale red (−0.4%) to blue (+0.4%) with present-day continents. Interpreted slabs are outlined in purple: Far, Farallon; Aeg, Aegean Tethys; MO, Mongol-Okhotsk. **b**, Unmodified reconstruction at 160 Myr. Offsets exist between the three slabs (purple) and their corresponding subduction complexes/sutures (red outlines). **c**, To obtain an improved fit between subduction complexes/sutures (green) and slab locations (purple), the plate tectonic reconstruction was shifted 18° westward.

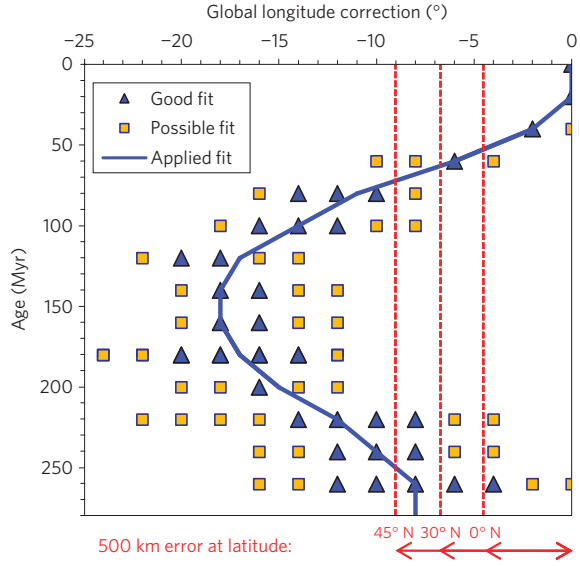

Figure 3 | Longitude correction with time. The blue triangles note a good global fit between slabs and continental plate margins. The orange squares note fits where some slabs are offset to the margins. The blue line represents the applied longitude correction to the plate tectonic reconstruction, based on the moving average of good global fits. The red dashed lines and arrows indicate the uncertainty, varying with latitude, to a lateral uncertainty of 500 km in the surface location of a palaeo-subduction zone.

mantle. The numerical mantle flow model[27] however, is based on mid-mantle observation and subducting continuous slabs, whereas our survival time estimate pertains to the lowermost mantle and detached slab remnants.

Tomographic invisibility can be caused by thermal assimilation, and/or mantle mixing, for example, by recycling in mantle plumes as indicated by geochemical signatures[28]. Recycling times of subducted oceanic lithosphere can be as short as a few hundred million years as indicated in the isotope geochemistry of some mantle plumes[29,30]. These short recycling times suggest that the deepest slab remnants may be the elusive source of recycled slab material observed in plumes, mixed with components of up to Archaean age[29]. Our observation of tomographic invisibility provides new input for future thermochemical dynamic modelling studies of slab survival in the deepest mantle.

To illustrate the implications for palaeo-longitude shifts of continents back to the Permo–Triassic, we use a plate tectonic reconstruction[3], recently corrected for true polar wander[4] between 100 and 300 Myr. From 12 depth slices in the lower mantle, corresponding to subduction during the time frame 40–260 Myr (Supplementary Figs S29–S40), we determine the shift of palaeo-longitudes of continental blocks from the inferred palaeo-subduction zone positions of the 28 slab remnants. As an example, we show how the three anchor slabs[8,9,11] constrain the plate tectonic reconstruction[3,4] (Fig. 2). A depth slice at 1,900 km in the tomographic model[7] corresponds to ~160 Myr of the plate tectonic reconstruction (Fig. 1). The unmodified reconstruction shows the Mongol-Okhotsk slab[9] to be located below central Asia, the Aegean Tethys slab[11] below central Europe and the Farallon slab[8] to be completely below the eastern Panthalassa Ocean (Fig. 2). All slabs are positioned too far west with respect to the subduction location inferred by the geological record[8,9,11]. A 16°–18° westward shift of the reconstruction provides the best fit, between slab remnants at depth and the surface location of subduction. Clearly, some offsets remain between our palaeosubduction positions inferred from tomography and the modified plate tectonic construction (Fig. 2c). These discrepancies approach the uncertainties in the inferred surface location of palaeo-subduction with an estimated lateral spatial r.m.s. uncertainty of ~250–500 km resulting from the effects of unknown slab dip (~300–700 km), lower-mantle thickening of slabs (~200–400 km) and tomographic imaging error (~200–400 km) of the interpreted medium to well-imaged slab remnants. Other uncertainties are due to complexities in the slab subduction history, for example, the northern Farallon slab is related to subduction at the continental margin, but its southern extent may have been caused by simultaneous intra-oceanic subduction[20].

An important overall observation is that, at each time slice considered, the relative position of continental fragments in the plate reconstruction[3,4] proves largely consistent with our inferred relative positions of palaeosubduction zones (Fig. 2, Supplementary Figs S29–S40). This gives confidence in the plate reconstruction[3,4] used and in our inferred palaeo-subduction zone configurations. This also allows us to concentrate on longitude shifts per time slice of the entire assembly of continental fragments. These are summarized in Fig. 3, whereas Fig. 4 serves to illustrate our interpretation process. In Fig. 4 and Supplementary Figs S29–S40, we also speculate on the palaeo-position of intra-oceanic blocks, spreading ridges and transform zones, but this is not essential for our analysis of absolute palaeolongitude.

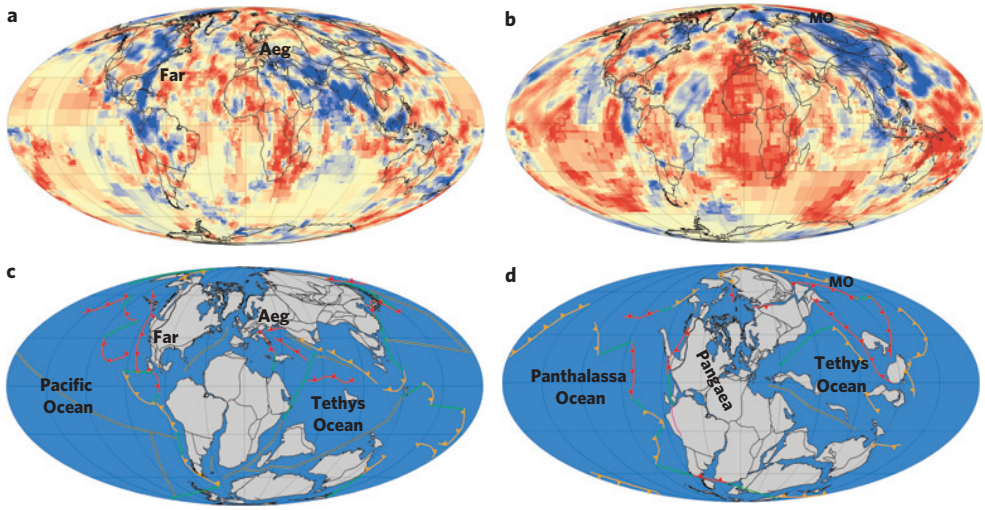

Figure 4 | Longitude-corrected plate tectonic reconstructions. The colour scale is given in Fig. 2 and slab name abbreviations are given in Table 1. **a**–**d**, A good fit is obtained between the tomographic depth slices[7] at 1,325 km (**a**) and 2,650 km (**b**) depth and the modified plate tectonic reconstructions[3,4] at 120 Myr (17° corrected) (**c**) and 240 Myr (10° corrected) (**d**). Tectonic interpretation: lines with triangles, subduction zone of the slab data set (red) and other slabs with only a qualitative interpretation (orange); green line, transform zone; yellow double line, spreading ridge. See Supplementary Figs S29–S40 for larger maps.

On the basis of slab remnants between 45° N and 45° S, we find that palaeolongitudes gradually depart between 40 and 120 Myr, amounting to a westward longitude shift of 18°–20° between 120 and 180 Myr, after which a gradual decrease occurs to 8° at 260 Myr (Fig. 3). Owing to uncertainties, this departure is significant from ~80 to ~260 Myr and provides new constraints on the palaeolongitude of the entire continental-plate configuration through time. Figure 4 shows that the continents on the Northern Hemisphere are constrained by slabs on either side of the palaeo-Pacific Ocean (for example, Farallon slab[8]) and by Tethys Ocean slabs (for example, Aegean Tethys slab[11]). The longitude correction decreases to ~10° in the Late Permian–Triassic (200–260 Myr). Bordered by slabs at its western and eastern side (for example, Mongol-Okhotsk slab[9]), Pangaea is also constrained in absolute longitude (Fig. 4).

Our global atlas of subduction remnants agrees through geological time with the relative positions of continental plates and agrees within 18°–20° with the palaeolongitude of the entire continental assembly as given by the plate reconstruction[3,4] used for comparison. The latter reconstruction also proposes absolute palaeo-longitudes of continental plates[17]. Given the uncertainties underlying both approaches, we have obtained a rather close match between independently proposed palaeolongitudes through time. The required longitude corrections do not significantly affect the correlation between mantle heterogeneities at the core–mantle boundary and large igneous provinces[17].

The longitude correction pattern of Fig. 3 may reflect Pangaea (Africa) wandering in longitude, but does require further investigation, eventually leading to an integration of both approaches and a further quantification of plate reconstructions. Here, we have focused on new inferences on absolute plate motion, lower-mantle sinking rates and the tomographic visibility of slab remnants, potentially useful as constraints on mantle rheology and on geodynamic modelling of crust–mantle evolution.

Methods

We selected only imaged anomalies in the UU-P07 tomographic model[7], with peak velocity amplitudes above +0.4%, and overall amplitudes above +0.2% to delineate slab boundaries[12]. Subduction zones associated with large oceanic basins are expected to be of considerable lateral extent; therefore, the interpretation is further restricted to laterally elongated deep-mantle anomalies, leading to the data set of 28 slab remnants (Table 1). The Supplementary Information provides our global atlas of slab remnant interpretations, which may prove useful for future tomographic and plate tectonic studies. The radial error in the depth interpretation varies from ±100 km in the shallow lower mantle to ±200 km in the deeper lower mantle.

The set of 28 slabs is subdivided into three confidence categories. Category I slabs have previously been interpreted in tomographic studies and correlated to their respective orogens[8–13]. Age uncertainties are derived from geological literature. Vertical spatial uncertainties are conservative (upper) estimates of image blurring effects.

Slabs in category II are found in the vicinity of a category I slab, providing a palaeogeographic link to the latter, assuming they have been created and shaped in the same boundary region between two converging plates. Candidates for corresponding orogens are identified from palaeo-geographic reconstructions[5,19–21], which are primarily determined from the synthesis of geological and palaeo-magnetic data. For slabs of category III, there is no apparent relation with other slabs, or the interpretation of subduction remnants has led to relatively larger uncertainties in subduction timing and depth as compared with the first two categories.

The initial identification of category II and III slabs from palaeo-geographic reconstructions is tied in with the interpretations of category I slabs. The subsequent estimates for top and bottom depth from the tomographic model and the more precise timing of start and end of subduction from the geological literature are independent of this initial identification process.

To test the data-set robustness, the time–depth data set is split in various ways: separately considering the top and base of slab remnants (Supplementary Fig. S41), per slab remnant confidence category (Supplementary Fig. S42) and per region (Supplementary Fig. S43).

The longitude correction was estimated by correlating the plate tectonic reconstruction in 20 Myr steps with the closest available depth slice (tomographic layer), based on the average time–depth conversion as indicated by the slab data set. Global longitude shifts were applied in 2° steps and the fit quality was assessed between the active palaeo-margins at surface and slab remnants at depth. Latitudes of continental fragments were not changed, except for the North China block in the Permo–Triassic. Mesozoic Europe has been simplified by excluding small continental fragments at its southern margin. Where flat-slab orogenies occurred, the intra-plate edge of crustal deformation was taken to match the dispersed slabs remnants. Locations of spreading ridges and transform zones have also been added, but are based on speculation.

Received 10 June 2009; accepted 2 November 2009; published online 6 December 2009

References

1. Müller, R., Royden, J. & Lawver, L. Revised plate motions relative to the hotspots from combined Atlantic and Indian Ocean hotspot tracks. *Geology* **21,** 275–278 (1993).
2. Norton, I. *The History of Global Plate Motions* 339–357 (Geophysical Monograph Vol. 121, 1996).
3. Torsvik, T., Müller, R., van der Voo, R., Steinberger, B. & Gaina, C. Global plate motion frames: Toward a unified model. *Rev. Geophys.* **46,** 1–44 (2008).

4. Steinberger, B. & Torsvik, T. Absolute plate motions and true polar wander in the absence of hotspot tracks. *Nature* **452,** 620–624 (2008).
5. Stampfli, G. & Borel, G. D. *The TRANSMED Transects in Space and Time: Constraints on the Paleotectonic Evolution of the Mediterranean Domain: The TRANSMED Atlas* Ch. 3 (Springer, 2004).
6. Scotese, C. *Atlas of Earth History* (PALEOMAP Project, 2001).
7. Amaru, M. *Global Travel Time Tomography With 3-D Reference Models, Geol. Traiectina*. PhD thesis, Utrecht Univ. 1–174 (2007).
8. Grand, S., van der Hilst, R. & Widiyantoro, S. Global seismic tomography: A snapshot of convection in the earth. *GSA Today* **7,** 1–7 (1997).
9. van der Voo, R., Spakman, W. & Bijwaard, H. Mesozoic subducted slabs under Siberia. *Nature* **397,** 246–249 (1999).
10. van der Voo, R., Spakman, W. & Bijwaard, H. Tethyan slabs under India. *Earth Planet. Sci. Lett.* **171,** 7–20 (1999).
11. van Hinsbergen, D., Hafkenscheid, E., Spakman, W., Meulenkamp, J. & Wortel, M. Nappe stacking resulting from subduction of oceanic and continental lithosphere below Greece. *Geology* **33,** 325–328 (2005).
12. Hafkenscheid, E., Wortel, M. & Spakman, W. Subduction history of the Tethyan region derived from seismic tomography and tectonic reconstructions. *J. Geophys. Res.* **111,** B08401 (2006).
13. Sigloch, K., McQuarrie, N. & Nolet, G. Two-stage subduction history under North America inferred from multiple-frequency tomography. *Nature Geosci.* **1,** 458–462 (2008).
14. Schellart, W., Kennett, B., Spakman, W. & Amaru, M. Plate reconstructions and tomography reveal a fossil lower mantle slab below the Tasman Sea. *Earth Planet. Sci. Lett.* **278,** 143–151 (2009).
15. De Jonge, M., Wortel, M. & Spakman, W. From tectonic reconstruction to upper mantle model: An application to the Alpine–Mediterranean region. *Tectonophysics* **223,** 53–65 (1993).
16. Hall, R. & Spakman, W. Subducted slabs beneath the eastern Indonesia-Tonga region: Insights from tomography. *Earth Planet. Sci. Lett.* **201,** 321–336 (2002).
17. Torsvik, T., Steinberger, B., Cocks, L. & Burke, K. Longitude: Linking Earth's ancient surface to its deep interior. *Earth Planet. Sci. Lett.* **276,** 273–282 (2008).
18. Steinberger, B. Slabs in the lower mantle—results of dynamic modelling compared with tomographic images and the geoid. *Phys. Earth Planet. Inter.* **118,** 241–257 (2000).
19. Golonka, J. *et al.* Paleogeographic reconstructions and basins development of the Arctic. *Mar. Petrol. Geol.* **20,** 211–248 (2003).
20. Nokleberg, W. *et al.* Phanerozoic tectonic evolution of the circum-north Pacific. *USGS Professional Paper* 1626 (2000).
21. Cawood, P. & Buchan, C. Linking accretionary orogenesis with supercontinent assembly. *Earth Sci. Rev.* **82,** 217–256 (2007).
22. Bijwaard, H., Spakman, W. & Engdahl, E. Closing the gap between regional and global travel time tomography. *J. Geophys. Res.* **103,** 30055–30078 (1998).
23. Liati, A., Gebauer, D. & Fannink, C. The age of ophiolitic rocks of the Hellenides (Vourinos, Pindos, Crete): First U-Pb ion microprobe (SHRIMP) zircon ages. *Chem. Geol.* **207,** 171–188 (2004).
24. DeCelles, P., Ducea, M., Kapp, P. & Zandt, G. Cyclicity in Cordilleran orogenic systems. *Nature Geosci.* **2,** 251–257 (2009).
25. van der Lee, S. & Nolet, G. Seismic image of the subducted trailing fragments of the Farallon plate. *Nature* **386,** 266–269 (1997).
26. Ricard, Y., Richards, M., Lithgow-Bertollini, C. & Le Stunff, Y. A geodynamic model of mantle density heterogeneity. *J. Geophys. Res.* **98,** 21895–21909 (1993).
27. Jarvis, G. & Lowman, J. Survival times of subducted slab remnants in numerical models of mantle flow. *Earth Planet. Sci. Lett.* **260,** 23–36 (2007).
28. Chauvel, C., Lewin, E., Carpentier, M., Arndt, N. & Marini, J. Role of recycled oceanic basalt and sediment in generating the Hf–Nd mantle array. *Nature Geosci.* **1,** 64–70 (2008).
29. Schaefer, B., Turner, S., Parkinson, I., Rogers, N. & Hawkesworth, C. Evidence for recycled Archaean oceanic mantle lithosphere in the Azores plume. *Nature* **420,** 304–307 (2002).
30. Hauff, G., Hoernle, K., Tilton, G., Graham, D. & Kerr, A. Large volume recycling of oceanic lithosphere over short timescales: Geochemical constraints from the Caribbean Large Igneous Province. *Earth Planet. Sci. Lett.* **174,** 247–263 (2000).

Acknowledgements

We would like to thank the various people of Shell in Rijswijk, the Netherlands, for the valuable discussions on regional geology, A. Crince for technical support and R. Hall and P. Cawood for fruitful comments. Part of this work was conducted under programmes of the Vening Meinesz School of Geodynamics (VMSG, Utrecht University) and the Netherlands Research Centre of Integrated Solid Earth Sciences (ISES). D.J.J.v.H. acknowledges an NWO-VENI grant. This paper contributes to the ESF EUROCORES programme TOPO-EUROPE.

Author contributions

D.G.v.d.M. carried out the global tomographic slab identification, longitude correction and plate tectonic reconstruction modifications, partly during his sabbatical at the NGU. W.S. co-developed the tomographic model and the ideas underlying the research presented here. D.J.J.v.H. provided integration between surface geology, orogenesis and subduction. M.L.A. developed the tomographic model as part of her PhD work at Utrecht University. T.H.T. provided the plate tectonic reconstructions. The first three authors shared equally in writing the article.

Additional information

The authors declare no competing financial interests. Supplementary information accompanies this paper on www.nature.com/naturegeoscience. Reprints and permissions information is available online at http://npg.nature.com/reprintsandpermissions. Correspondence and requests for materials should be addressed to D.G.v.d.M. or W.S.